

The effects of forcing and dissipation on phase transitions in thin granular layers.

Alexander E. Lobkovsky¹, Francisco Vega Reyes², and J. S. Urbach^{3,a}

¹ National Institutes of Health, Bethesda, MD 20894

² Departamento de Física, Universidad de Extremadura, E-06071 Badajoz, Spain

³ Department of Physics, Georgetown University, Washington DC, 20057

Abstract. Recent experimental and computational studies of vibrated thin layers of identical spheres have shown transitions to ordered phases similar to those seen in equilibrium systems. Motivated by these results, we carry out simulations of hard inelastic spheres forced by homogenous white noise. We find a transition to an ordered state of the same symmetry as that seen in the experiments, but the clear phase separation observed in the vibrated system is absent. Simulations of purely elastic spheres also show no evidence for phase separation. We show that the energy injection in the vibrated system is dramatically different in the different phases, and suggest that this creates an effective surface tension not present in the equilibrium or randomly forced systems. We do find, however, that inelasticity suppresses the onset of the ordered phase with random forcing, as is observed in the vibrating system, and that the amount of the suppression is proportional to the degree of inelasticity. The suppression depends on the details of the energy injection mechanism, but is completely eliminated when inelastic collisions are replaced by uniform system-wide energy dissipation.

1 Introduction

Excited granular materials show a variety of interesting non-equilibrium phenomena that raise important fundamental and practical questions [1]. Studies on steady states of simple model systems comprised of identical, spherical, non-cohesive inelastic spheres have proven to be valuable for developing and testing extensions of statistical mechanics to non-equilibrium systems. Measurements of velocity distributions have revealed significant deviations from equilibrium Maxwellian distribution function [2,3,4,5,6,7,8], and velocity correlations show violations of molecular chaos [9]. These observations are reasonably well described by non-equilibrium kinetic theory, which shows that non-equilibrium effects arise from the mechanism of energy injection [10,11,12].

While the ‘microscopics’ of inelastic particles differs significantly from their equilibrium analogs, the macroscopic phase behavior of non-equilibrium steady states of excited granular media can show remarkable similarity to equilibrium systems. The crystallization of a single layer of vibrated spheres into a hexagonally ordered array can be directly mapped onto the analogous 2D phase transition [13,14]. In the presence of a confining lid, we have reported a complex phase diagram that is closely related to that observed in similarly confined equilibrium colloidal systems, including two-layer crystals with square or hexagonal symmetry [15,16,17]. In a recent study Clerc et al. [18] extended this work to quasi-one-dimensional systems, and showed that the transition to an ordered phase was mediated by traveling waves and was triggered

^a e-mail: urbach@physics.georgetown.edu

by negative compressibility. However, in spite of the strong similarities between the phase diagrams of equilibrium and granular systems, experimental observations indicate that phase transitions in granular systems exhibit a richer and more complex behavior. There are ordered phases that arise solely from nonequilibrium effects, such as the hexagonal collapse observed in granular monolayers at low vibration amplitudes [2]. Experimental and computational studies have shown that inelasticity suppresses the transition to the ordered phase [17,18], but the mechanism of this suppression is still not well understood.

Motivated by these results, we have performed computational studies of identical, spherical, inelastic spheres in a quasi-2D geometry, excited either by random forces or by external vibration. The transition to the ordered phase in the randomly driven system is suppressed when inelasticity is increased, as in the vibrated system. However, unlike spheres under vibration, there is no clear phase separation in the case of random driving. We show that the energy injection in the vibrated system is strongly phase-dependent, and suggest that this dependence creates an effective surface tension that accounts for the strong phase separation observed under vibration. In addition, we show that the suppression of the ordered phase in the randomly driven system depends in a non-trivial way on both the form of the energy injection and the form of the dissipation.

2 Computational methods

We report results from two simulation techniques: soft sphere molecular dynamics used to simulate the experiments with external vibration, and hard sphere event driven simulations with random energy injection. In all cases we simulate thin granular layers, with identical spherical particles in a three dimensional domain that has periodic boundary conditions in two dimensions (simulating the horizontal plane in the vibrating plate experiments). In the third (‘vertical’) dimension, the spheres are confined to a space of 1.75σ , where σ is the sphere diameter. A constant gravitational acceleration is included in the simulations of vertical vibrations, but not the random driving simulations.

2.1 Soft sphere molecular dynamics simulations of vertical vibrations

We simulate the vertical vibration of the experiments by imposing a sinusoidal oscillation on the horizontal boundaries with amplitude A and frequency ν (keeping the spacing between the boundaries fixed). We have used a collisional model of rough (the particles have rotational kinetic energy), soft (there is particle-particle overlap during collisions) inelastic (collisions are dissipative) spheres. The collisions are characterized by three forces. Two forces are normal to the direction of collision, one is an elastic restoring force \mathbf{F}^{rest} , proportional to particle/particle overlap, and the other is a frictional dissipative force \mathbf{F}^{diss} , proportional to relative normal velocity. The third force $\mathbf{F}^{\text{shear}}$, which is tangential, is also frictional and dissipative (inelastic). The same types of forces are used for particle-wall collisions (there is also particle-wall overlap during these collisions). The interactions included in the model do not capture the full complexity of real inelastic collisions [19], but do reproduce the dominant effects of vibration, collisions, and dissipation. Furthermore, this collisional model has successfully reproduced a wide variety of phenomena that are observed in experiments, including pattern formation [20], clustering [21], rheological behavior [22], impurity segregation [23], velocity correlations [9], depletion forces [24] and phase transitions [15,16]. Moreover, simulations with this collisional model reproduce our experimental observations that ordered phases are suppressed in highly inelastic materials [17].

The wall-particle forces can be expressed as

$$\mathbf{F}_{iw}^{\text{rest}} = Y_w m_i (|\mathbf{r}_{iw}| - \sigma) \hat{\mathbf{r}}_{iw}, \quad \mathbf{F}_{iw}^{\text{diss}} = -\gamma_{nw} m_i \mathbf{v}_{iw}^n, \quad \mathbf{F}_{iw}^{\text{shear}} = -\gamma_{sw} m_i \mathbf{v}_{iw}^t. \quad (1)$$

The particle-particle interactions have analogous forms

$$\mathbf{F}_{ij}^{rest} = Y m_i (|\mathbf{r}_{ij}| - \sigma) \hat{\mathbf{r}}_{ij}, \quad \mathbf{F}_{ij}^{diss} = -\gamma_n m_i \mathbf{v}_{ij}^n, \quad \mathbf{F}_{ij}^{shear} = -\gamma_s m_i \mathbf{v}_{ij}^t, \quad (2)$$

In the above equations (1, 2), subscripts a, b may be w , which stands for the walls, or i, j , which stand for particles; m_i is the particle mass; \mathbf{r}_{ab} are relative positions: $\mathbf{r}_{ab} = \mathbf{r}_a - \mathbf{r}_b$, and $\hat{\mathbf{r}}_{ab} = \mathbf{r}_{ab}/|\mathbf{r}_{ab}|$. Analogously, \mathbf{v}_{ab} stands for relative velocities, and $\mathbf{v}_{ab}^n, \mathbf{v}_{ab}^t$ stand for the projections of relative velocities in the normal and tangential directions respectively. The coefficient Y is the Young modulus that characterizes the restoring force whereas γ_n, γ_s account for the dissipation in the normal and tangential directions respectively. In this work we have used values of parameters that mimic the behavior of metallic balls with a coefficient of normal restitution $\alpha \sim 0.87$ [23], which is an intermediate value between the experimental values $\alpha = 0.95$ and $\alpha = 0.77$ for steel and brass spheres [17]. We have used the same values of force parameters for the wall-particle interactions. Specifically, we use $Y = Y_w = 10^7 \text{ s}^{-2}$, $\gamma_n = \gamma_{nw} = 200 \text{ s}^{-1}$, $\gamma_s = \gamma_{sw} = 200 \text{ s}^{-1}$.

In order to calculate the energy input from the vibrating plate, we define the magnitude

$$W_{in} = \left| \sum_i^{bin} (\mathbf{F}_{iw} \cdot \mathbf{v}_i dt + (\mathbf{r}_{iw} \times \mathbf{F}_{iw}) \cdot \frac{d\boldsymbol{\omega}_i}{dt} dt) \right| \quad (3)$$

(with dt the time step in the simulation, $\boldsymbol{\omega}_i$ the particle angular velocity, and $\mathbf{F}_{iw} = \mathbf{F}_{iw}^{rest} + \mathbf{F}_{iw}^{diss} + \mathbf{F}_{iw}^{shear}$). In order to produce the profiles shown below, W_{in} is averaged in steady states over small square bins of the size of less than $\sigma/2$ and a time interval $\Delta t \sim 10 \text{ s}$.

2.2 Event driven hard sphere simulations of random driving

We simulate frictionless, smooth hard spheres using event driven simulations [25]. We implemented a reduced collision list version of the event driven algorithm in which the simulation box is divided into cells and only collisions between pairs of particles in neighboring cells are considered. We do not employ sophisticated data structures for the schedule of events and simply keep an ordered list of collisions and cell boundary crossings.

When either the interparticle coefficient of restitution e or particle-wall coefficient of restitution e_{wall} is less than unity, energy must be supplied to the system to balance the energy dissipated in collisions. We consider three ways of injecting energy, which we term global kicking, local kicking and hot-wall.

When the ‘‘global kicking’’ is in use, at every particle collision we select a random particle pair distinct from the colliding pair and give the selected particles equal and opposite velocity kicks drawn from a normal distribution with zero mean. The ‘‘local kicking’’ method draws pairs of particles from neighboring cell. This method may reduce the long wavelength velocity correlations that arise from random pair kicking [33]. In the vibrating system, the energy injection occurs only when particles collide with the top and bottom boundaries. To mimic this feature of the vibrated system, we implemented what we call the ‘‘hot-wall’’ driving. A kick in the X - Y (‘‘horizontal’’) plane is administered to a particle which collides with a confining plate. The magnitude of the kick is saved and a kick equal in magnitude and opposite in direction is administered to the next particle which undergoes a collision with a confining plate. The pairwise administration of kicks assures that the center of mass momentum does not grow without bound [26].

To study the importance of inelastic collisions on ordering we also implemented a ‘‘global energy sink’’ with elastic ball-ball and ball-wall collisions. The energy injected by the random kicks is removed by rescaling particle velocities by a constant factor after every kick to keep the total kinetic energy constant. Because all velocities are rescaled by the same factor, all events in the list are still valid modulo an appropriate rescaling of the event times. The standard deviation of the kicking velocity distribution, v_{kick} , relative to the fixed total kinetic energy, combined with the number of kicks per collision, determines how different the system is from the elastic system.

To test for the appearance of the phase consisting of two layers with square symmetry, we calculate the order parameter, Ψ_8 , which measures the degree of square order in the X - Y plane. It is defined as

$$\Psi_8 = \frac{1}{N} \left| \sum_{i=1}^N \psi_i^8 \right|, \quad \psi_i^8 = \frac{1}{n_i} \sum_{\langle j \rangle} e^{8\pi I \theta_{ij}}, \quad (4)$$

where $I = \sqrt{-1}$, the sum over $\langle j \rangle$ in the definition of ψ_i^8 is over n_i neighbors of i defined as those spheres whose center is within a cutoff distance 1.35σ in the X - Y plane from the center of i and θ_{ij} is the angle between the X - Y projection of $\mathbf{r}_i - \mathbf{r}_j$ and the X axis. When the system is perfectly ordered into a square lattice in the X - Y plane, $\Psi_8 = 1$, whereas a randomly positioned collection of spheres has $\Psi_8 \sim 1/\sqrt{N}$.

3 Vibrated layers

The simulations described in this paper were motivated by a series of experimental results on a system consisting of a collection of identical spherical particles on a horizontal plate vibrating vertically, with a confining lid [15,16,17]. This system is well suited to investigate many of the complex non-equilibrium effects observed in excited granular media and is simple enough that it can be accurately modeled in molecular dynamics simulations [15].

3.1 Phase Diagram

The vibrated system shows a wide variety of steady states, depending on the number of particles, the vibration frequency and amplitude, and the gap between the plate and the confining lid [15,16,17,18]. For the gap spacing studied here (1.75σ), the spheres spontaneously organize into a two-layer ordered phase showing square symmetry. The ordered phase forms at sufficiently high density, and is observed for a range of vibration amplitudes and frequencies. At slightly larger gaps, the spheres form a two layer hexagonally ordered phase, while at smaller gaps a variety of complex phases are observed [16]. This surprising behavior can be understood, at least in part, by considering the very similar behavior observed in equilibrium hard sphere colloidal suspensions confined in a similarly narrow gap [27]. These systems show a complex phase diagram that depends on the volume fraction of the colloidal particles and the ratio of the confining gap to the particle diameter [27,28,29,30,31,32]. The phase diagram can be explained in terms of entropy maximization. The configuration that gives the particles the most room to rattle around, within the constraints imposed by the gap, will minimize the free energy of the system. It remains unclear, however, whether this picture can be extended to explain the non-equilibrium steady states observed in the granular layer. In the next two sections we describe purely non-equilibrium effects that are not present in the colloidal suspensions.

3.2 Phase dependence of energy injection

For a range of densities, the two-layer square phase coexists with a disordered liquid-like phase, with a sharp boundary between the phases. The square phase has a much higher density (nearly close packed) and much lower granular temperature than the surrounding liquid [15]. As described in Section 4, these effects are not present in systems of elastic spheres or of randomly driven inelastic spheres, although the square phase is observed at high densities. One important feature of energy injection by vibration that is not present in many idealized models of granular forcing is that the rate of energy injection depends on the local dynamics of the system. We performed molecular dynamics simulations to directly measure the rate of energy flow from the vibrating plate to the two coexisting phases.

Fig 1a shows a color map of the local average rate of energy input. Superimposed on the colormap are crosses representing the instantaneous position of the spheres. The square phase

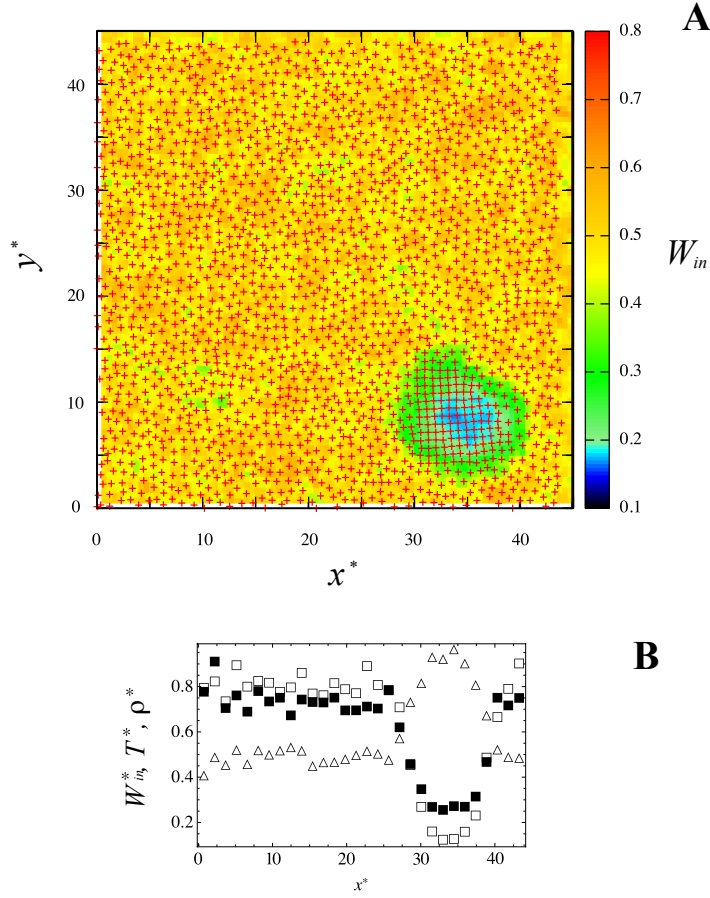


Fig. 1. Energy injection in vibrated system is phase-dependent. **A.** The color map shows the square of the energy input, W_{in} , as defined in Eq. 3, with $x^*, y^* = x/\sigma, y/\sigma$. The position of the center of each ball at the midpoint of the averaging period is marked with +. The dramatic reduction in energy input in the lower right corner coincides with the ordered phase. **B.** Normalized profiles of energy input W_{in}^* (■), horizontal granular temperature T_h^* (□) and density ρ^* (△). The normalization is calculated according to $a^*(x) = a(x)/a_{max}$, where a_{max} is the maximum value of a in the system. The profiles are measured along a straight line passing through the center of the ordered phase. (N=2000, system size $L = 44 \sigma$, gap spacing $h = 1.75 \sigma$ ($\sigma = 1.19063$ mm) vibration frequency $\nu = 60$ Hz, input acceleration $\Gamma = A(2\pi\nu)^2/g = 3.00$ ($g = 9.80$ ms $^{-2}$). Plots result from averaging over 10 s.)

is clearly visible, and exactly coincides with a region of dramatically reduced energy input. In order to more clearly show the correspondence, we show in Fig. 1b the normalized energy input rate (solid squares), granular temperature (open squares), and density (triangles), calculated for a narrow strip that runs through the center of the ordered phase. The implications of these results are discussed in Section 6.

3.3 Effects of inelasticity

We recently reported the existence of a melting transition of the square ordered phase as the vibration amplitude is increased, both in experiments and computer simulations [17]. Furthermore, experiments showed that the melting of the crystalline phase occurs significantly earlier

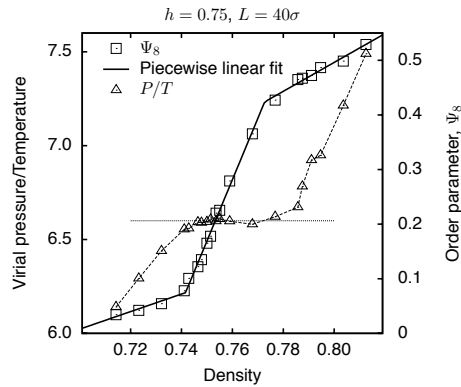


Fig. 2. Virial pressure scaled by the temperature (triangles) measured in a series of constant volume simulations of elastic spheres shows a plateau as a function of density indicative of a coexistence between two phases. The square order parameter Ψ_8 (squares) exhibits a rapid growth rate in the same density window. A piece-wise linear fit to Ψ_8 yields the densities bracketing the coexistence region.

in brass spheres than in less inelastic stainless steel spheres, and computer simulations showed that the ordered phase is not present at any vibration amplitude when the inelasticity is large. A reduction in the liquid-solid coexistence region at fixed vibration amplitude was also observed in computer simulations in [18]. These results indicate that ordering is suppressed by inelasticity and that the strength of dissipation can qualitatively alter the phase diagram of even the simplest granular media. One of the motivations for the work described here is to see if that effect is unique to vibrated granular systems.

4 Randomly driven layers

In order to elucidate the effects of forcing and dissipation on the phase diagram, we performed simulations on randomly driven hard spheres. Although there is no experimental system that closely matches the random driving, it has a number of advantages relative to the vibrated system. For a given geometry, the state of the system is fully specified by density and inelasticity, whereas amplitude and frequency are also relevant parameters for the vibrated system. The behavior of the randomly driven hard spheres can be compared with equilibrium hard sphere suspensions by observing the behavior as e approaches unity.

4.1 Elastic hard spheres

Elastic hard spheres confined to a gap of 1.75σ undergo a transition from disorder (liquid) to square order (crystal) upon increasing density [27,28,29,30,31,32]. At constant volume, the two phases coexist in a range of densities. The signature of coexistence is a plateau in the pressure as a function of density. Figure 2 shows the virial pressure scaled by the temperature (which is constant in an elastic, constant volume system) as a function of density, defined as $AH/(N\sigma^3)$, where $A = L^2$ is the area of the confining plates. The plateau is indicative of coexistence between the densities of roughly 0.75 and 0.77.

Another signature of the phase coexistence is found by examining the variation of the order parameter Ψ_8 with density. In the coexistence region, the system presumably separates into two distinct regions characterized by different order parameters. Since the characteristic densities of the phases should remain the same in the coexistence region, the fraction of the system in the ordered state grows linearly from 0 to 1 as the density increases. The mean order parameter averaged over the whole system should therefore exhibit a linear increase as well. As shown in Figure 2, an estimate of the boundaries of the coexistence region determined from piecewise

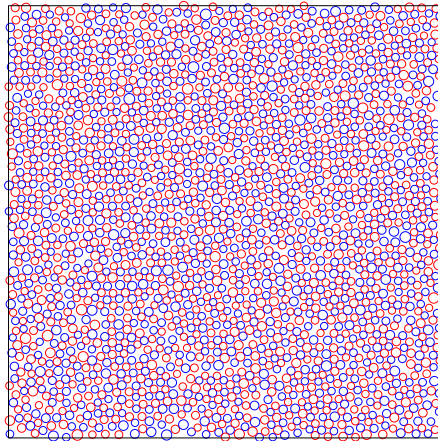


Fig. 3. Snapshot of the $z = H/2$ section through the elastic system in the coexistence region. The density is $\rho = 0.768$, $L = 40\sigma$ and $h = 1.75\sigma$. The larger circles result from spheres with centers closer to the $z = H/2$ plane, and the color indicates whether the center of a particular sphere is below (blue) or above (red) that plane.

linear fits to the order parameter vs. density curve is roughly consistent with the extent of the plateau in the pressure vs. density graph.

A snapshot of the elastic system at a density that is in the middle of the coexistence region is shown in Fig. 3. Unlike the vibrated inelastic system, there is no sharp separation between the ordered and disordered phases (compare with Fig. 1). We have looked extensively for indications of phase separation, including very long simulation runs and very large systems, but have always found a high degree of intermixing. Note that because this system is quasi-2D, it is perhaps not surprising that fluctuations dominate over what is presumably a very small effective surface tension. In the vibrated inelastic system, by contrast, the phase separation is dramatic, nearly instantaneous, and can be observed in both small and large systems [17].

4.2 Effects of Inelasticity

When particles are inelastic, energy must be continuously supplied to the system to maintain a dynamic steady state. We first focus on systems in which energy is supplied via the “global kicking” mechanism described in 2.2. Fig. 4A shows the order parameter vs. density for spheres with $e = e_{\text{wall}} = 0.9$. The data for elastic spheres (also shown in Fig. 2) is presented for comparison. As for the vibrated spheres, the transition to the ordered phase is shifted to a higher density in the inelastic system. The evolution of the transition region, determined piecewise linear fits to the order parameter vs. density curves, appears to be a smooth function of inelasticity, as shown in Fig. 4B. This suggests that the effect of the inelasticity can be thought of as a perturbation to the phase behavior of the elastic system. However, to our knowledge, there is no appropriate perturbation theory for the equilibrium statistical mechanical explanation of the transition to a state of square symmetry.

Images of the coexistence region in the inelastic system are indistinguishable from the elastic system. In particular, phase segregation between the ordered and disordered phases is never observed (unlike the vibrated system). Quantitative analyses of density-density and order parameter correlation functions show no features that clearly reveal effects of inelasticity, although our sensitivity is limited by the relatively small systems studied here.

Unlike the elastic system, plots of P or P/T vs. density do not, in general, show a plateau in the coexistence region (see Fig. 2). In the inelastic system, the steady state granular temperature is determined by the balance between forcing and dissipation. Thus the temperature will change if the configuration of the system changes, even if all parameters are kept constant. For a

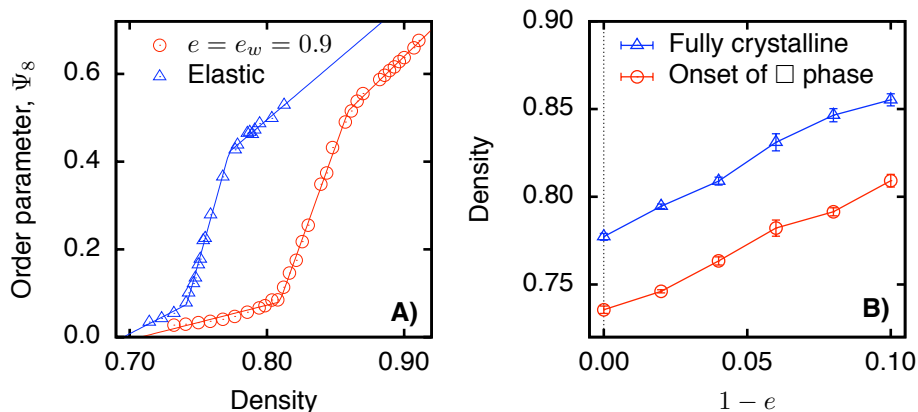


Fig. 4. **A)** The square order parameter in an elastic system compared to that of an inelastic system driven by random pair kicking (the global kicking method). The extracted boundaries of the coexistence region are plotted in panel **B)** as a function of sphere inelasticity e for a globally kicked system (wall inelasticity $e_{\text{wall}} = e$).

homogeneous hard sphere system, P/T should be independent of temperature, but we do not find a coexistence plateau in P/T . We hypothesize that this is because the temperature is non-uniform in the inelastic system. Even though the energy injection is homogeneous, denser regions will dissipate energy more quickly. Thus we expect that the ordered phases will be cooler, although the difference is more subtle than in the vibrated system and does not seem to yield a readily observable correlation between the temperature and order parameter.

5 Effect of forcing and dissipation

The results from the vibrated and randomly driven systems show that inelasticity suppresses the ordering transition, but the mechanism for the suppression is not well understood. In order to distinguish the relative importance of energy injection vs. energy dissipation, we performed simulations with different methods for energy input and energy dissipation. The results, summarized in Figure 5, are discussed below.

The pair kicking injection methods produce long-lived velocity correlations. (Ref. [33] studies the correlations that arise as a result of the “global kicking” method.) Picking the kicked pair from neighboring cells reduces, but does not altogether eliminate, the velocity correlations. Although we have not conducted a careful study of the “hot wall” driving, it too is likely to introduce long range velocity correlations, albeit of a different nature. Fig. 5A shows that for the same inelasticity “hot wall” driving (\triangle) suppresses square ordering the most, while the suppression for global (\odot) and local (\square) kicking are comparable, with the local kicking being the least effective at suppressing square order.

We employed the velocity rescaling “global energy sink” described in 2.2 to help to separate the effects of forcing from the effects of dissipation. Whereas collisions are elastic, the particles are given random kicks according to each of the three driving schemes, and the injected energy is removed “globally”. The order parameter-density curves, shown in Fig. 5B, are indistinguishable from the elastic case. This surprising result suggests that velocity correlations or other effects due to driving alone are not sufficient to suppress ordering.

In summary, we find that inelastic collisions suppress the transition to the ordered phase, and that the suppression is approximately proportional to the degree of inelasticity, but the exact amount of the suppression depends on the form of energy injection. In contrast, random kicking without inelastic collisions does not appear to significantly affect the location of the ordering transition.

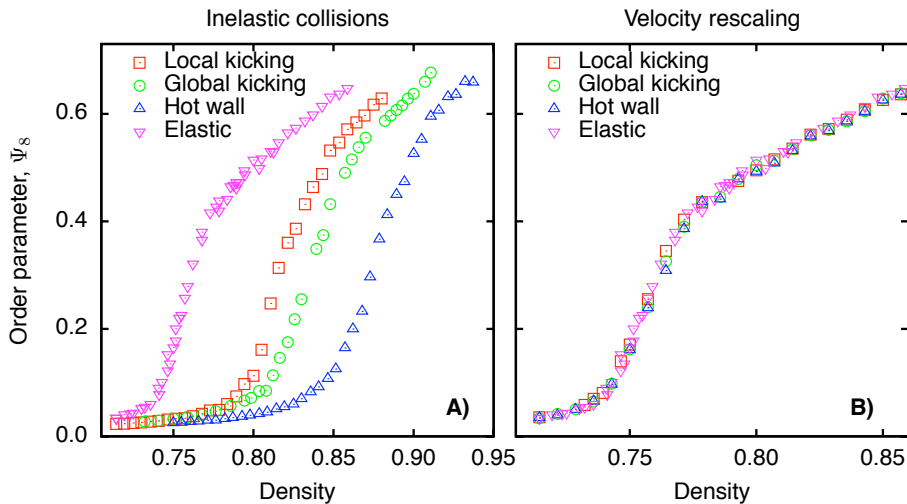


Fig. 5. The effect of different forms of energy injection and dissipation on the square ordering of the confined spheres. **A)** Order parameter vs. density for different forms of energy injection ($e = e_{\text{wall}} = 0.9$). **B)** Order parameter vs. density for global dissipation (velocity rescaling), with either local or global random kicking or a hot wall ($v_{\text{kick}} = 0.1 * \sqrt{2T}$).

6 Discussion

The results described in this paper provide several insights into the differences between phase transitions in excited granular layers and their equilibrium analogs, but also point to several unanswered questions.

Here we have shown directly that the energy flow from the vibrating plate into the dense ordered phase is much lower than into the surrounding dilute liquid. It has been shown previously that velocity-dependent driving can lead to clustering in driven granular monolayers [34], and is presumably the mechanism responsible for the 'collapse' observed in monolayers at small vibration amplitude [2]. Unlike the collapse, however, the ordered phases described in this paper are stable at high vibration amplitudes and occur at densities where elastic systems also show ordered phases. The absence of a clear phase separation between the ordered and disordered phases in confined elastic or randomly driven spheres suggests that the dramatic separation seen in the vibrated system can be traced to the inhomogeneous heating.

Our simulations of various forms of randomly driven hard spheres show that the suppression of the ordering transition upon increased inelasticity seen in vibrated layers is fairly generic, and that, at least for hard spheres, the transition evolves smoothly to the elastic limit as the inelasticity goes to zero. The significance of this result is that the phase transition in the weakly inelastic system should be explicable using the same machinery as the transition in the elastic case, which is driven by entropy maximization through geometric packing effects. However, non-equilibrium effects need to be included to explain how the phase boundaries shift with increasing dissipation.

The results from the simulations of different forms of random energy injection suggest a complex interplay between energy injection, dissipation, and ordering. The fact that the details of the forcing and dissipation will modify the location of the phase boundaries is perhaps not surprising. For example, the velocity correlations induced by the forcing could change the pressure in the disordered phase, which would likely shift the van der Waals instability that leads to the formation of the higher density phase. In this context the absence of any measurable shifts in the location of the ordering transition in simulations with random kicking and a global energy sink is perplexing.

While we have focused on somewhat idealized model systems, the effects are potentially relevant to a wide class of excited granular media. For most forms of energy injection, such as gas fluidization or shear flow, the local rate of heating will depend on the local state of the

granular media, as we have observed with the vibrated layers. The transition regime between a freely flowing granular liquid and rigid granular packing is critical in many situations, and the final steady state of a forced granular system will in general depend on the details of the balance between energy input and collisional cooling. A better understanding of the effects of forcing and dissipation on the transition in well controlled model systems will hopefully assist with the development of robust models for more complex systems.

7 Acknowledgments

This work was supported by NASA under award number NNC04GA63G. One of the authors (F. V. R.) acknowledges also support from Ministerio de Ciencia e Innovación (Spain) through contract No. FIS2007-60977 and Junta de Extremadura (Spain), through contract No. GRU09038.

References

1. I. S. Aranson, L. S. Tsimring, *Rev. Mod. Phys.* **78**, 641 (2006)
2. J. S. Olafsen, J. S. Urbach, *Phys. Rev. Lett.* **81**, 4369 (1998)
3. J. S. Olafsen, J. S. Urbach, *Phys. Rev. E* **60**, R2468 (1999)
4. W. Losert, D. G. W. Cooper, J. Delour, A. Kudrolli, J. P. Gollub, *Chaos* **9**, 682 (1999)
5. G. W. Baxter, J. S. Olafsen, *Nature* **425**, 680 (2003)
6. P. M. Reis, R. A. Ingale, M. D. Shattuck, *Phys. Rev. E* **75**, 051311 (2007)
7. G. W. Baxter, J. S. Olafsen, *Phys. Rev. Lett.* **99**, 028001(2007)
8. A. Burdeau, P. Viot, *Phys. Rev. E* **78**, 061306 (2009)
9. A. Prevost, D. A. Egolf, J. S. Urbach, *Phys. Rev. Lett.* **89**, 084301 (2002)
10. T. P. C. van Noije, M. H. Ernst, *Gran. Matt.* **1**, 57 (1998)
11. T. P. C. van Noije, M. H. Ernst, E. Trizac, I. Pagonabarraga, *Phys. Rev. E* **59**, 4326 (1999)
12. I. Pagonabarraga, E. Trizac, T. P. C van Noije, M. H. Ernst, *Phys. Rev. E* **65**, 011303 (2002)
13. J. S. Olafsen, J. S. Urbach, *Phys. Rev. Lett.* **95**, 098002 (2005)
14. P. M. Reis, R. A. Ingale, and M. D. Shattuck, *Phys. Rev. Lett.* **96** 258001 (2006)
15. A. Prevost, P. Melby, D. A. Egolf, J. S. Urbach, *Phys. Rev. E* **70**, 050301(R) (2004)
16. P. Melby, F. Vega Reyes, A. Prevost, R. Robertson, P. Kumar, D. A. Egolf, J. S. Urbach, *J. Phys. Cond. Mat.* **17**, S2689 (2005)
17. F. Vega Reyes, J. S. Urbach, *Phys. Rev. E* **78**, 051301 (2008)
18. M. G. Clerc, P. Cordero, J. Dunstan, K. Huff, N. Mujica, D. Risso, G. Vargas, *Nat. Phys.* **4**, 249 (2008)
19. S. F. Foerster, M. Y. Louge, H. Chang, H. Allia, *Phys. Fluids* **6**, 1108 (1994)
20. Rapaport, D. C. *The Art of Molecular Dynamics simulation.*, 2nd ed. (Cambridge University Press, 2004).
21. X. Nie, E. Ben-Naim, S. Y. Chen, *Europhys. Lett.* **51**, 679 (2000)
22. L. E. Silbert, D. Ertas, G. S. Grest, T. C. Halsey, D. Levine, S. J. Plimpton, *Phys. Rev. E* **64**, 051302 (2001)
23. J. Sun, F. Battaglia, S. Subramaniam, *Phys. Rev. E* **74**, 061307 (2006)
24. P. Melby, A. Prevost, D. A. Egolf, J. S. Urbach, *Phys. Rev. E* **76**, 051307 (2007)
25. T. Pöschel, T. Schwager, *Computational Granular Dynamics*, Ch. 3, Springer Verlag (2005)
26. C. Bizon, M. D. Shattuck, J. B. Swift, H. L. Swinney, *Phys. Rev. E* **60**, 4340 (1999)
27. B. Pansu, P. Pieranski, P. Pieranski, *J. Phys. (Paris)* **45**, 331 (1983)
28. P. Pieranski, L. Strzelecki, B. Pansu, *Phys. Rev. Lett.* **50**, 900 (1983)
29. B. Pansu, P. Pieranski, P. Pieranski, *J. Phys. (France)* **45**, 331(1984)
30. M. Schmidt, H. Löwen, *Phys. Rev. Lett.*, **76** 4552 (1996)
31. M. Schmidt, H. Löwen, *Phys. Rev. E* **55**, 7228 (1997)
32. R. Zangi, S. A. Rice, *Phys. Rev. E* **61**, 660 (2000)
33. A. Fiege, T. Aspelmeier, A. Zippelius, *Phys. Rev. Lett.* **102**, 098001 (2009)
34. R. Caferio, S. Luding, H. J. Herrmann, *Phys. Rev. Lett.* **84**, 6014(2000)